JOURNAL OF PROPULSION AND POWER
Vol. 26, No. 2, March–April 2010

Ultrasonically Aided Electrospray Source for Charged Particles Approaching Monodisperse Distributions

W. Song* and U. Shumlak†
University of Washington, Seattle, Washington 98195-2250

DOI: 10.2514/1.44257

A method of producing nearly monodisperse electrospray using charged capillary standing waves is investigated. The method, based on the ultrasonically aided electrospray concept, extracts charged particles from a liquid film with induced capillary standing waves at the critical stable condition by applying an electric field. Theoretical analysis on the formation of the charged particles is performed. An experimental ultrasonically aided electrospray system is designed and built to characterize the system operation and the resulting electrospray. The electrospray characterization includes Mie scattering and witness plate analysis. A mode of operation is found, in which the electric field dominates the electrospray production. The particle size and variation reduce with the applied electric field.

Nomenclature

A	=	wave amplitude
d	=	distance between electrodes
E	=	electric field
E_S	=	threshold electric field for direct charge emission
I	=	current
I_{sp}	=	specific impulse
j	=	current density in the electrospray
m	=	particle mass
P_e	=	pressure due to electrostatic forces
P_{st}	=	pressure due to surface tension
Q	=	liquid volume flow rate
q	=	particle charge
R_o, r_o, r	=	local radius of curvature of liquid meniscus
r_d	=	droplet radius
S	=	surface area
u	=	velocity
$\mathbf{V}$	=	voltage
V	=	volume
x	=	volume concentration of solid particles in suspension
α	=	angle
ε_0	=	permittivity of vacuum
Λ	=	axial wavelength of waves in liquid column
λ	=	wavelength of capillary waves in liquid surface
σ	=	surface tension coefficient
ρ	=	density
ω	=	angular frequency

I. Introduction

THE use of charged or uncharged nanoparticles can be found in many areas of scientific research, as well as industrial and engineering applications [1–4]. In the field of electrostatic space propulsion, particularly, heavy charged particles are often preferable to lighter atomic ions. For an electrostatic thruster operating at the space charge limited current density with a fixed exhaust velocity, a higher mass-to-charge ratio yields a higher thrust density. Therefore, the acceleration of heavier charged particles holds the promise of extending the useful range of electrostatic propulsion to a higher thrust power density. For example, existing ion engines, which use ionized gas as propellant and usually deliver a high specific impulse I_{sp}, are only able to produce low thrust density with a total thrust of usually less than 1 N. Such low thrust can be adequate for spacecraft orbit raising or position keeping, but it is not adequate for translating large spacecraft in space for deep space missions. If the mass-to-charge ratio of the charged species for an ion engine is increased, the thrust density (as well as the total thrust) increases substantially. For this reason, high molecular weight propellants (such as xenon) have been used in many ion engines. Because the mass-to-charge ratio of atomic ions is limited, researchers are turning their attention to heavy charged particles. Many of the heavy particles consisting of clusters of atoms, with the primary diameters less than 100 nm, are better known as nanoparticles. Therefore, producing uniformly charged and monodisperse nanoparticles with the appropriate charge-to-mass ratio is key to developing the next generation of high performance electrostatic thruster for advanced space missions that require a higher thrust level at an optimum I_{sp}.

Another interesting application area of charged or uncharged nanoparticles is in various nanotechnologies. Nanotechnologies are seen to have many industrial applications. The National Science Foundation (NSF) has predicted that the global market for nanotechnologies will reach $1 trillion or more within 20 years, most near-term (1–5 years) applications of nanotechnology are related to materials in the form of nanoparticles [3]. Many of these applications involve the aerospace field. At the nanometer scale, the physical, chemical, and biological properties of the materials differ in fundamental and valuable ways from the properties of individual atoms and the molecules or bulk matter. For example, a coating with nanoparticles can greatly improve the performance of bulk materials in many aspects, such as surface toughness, abrasion and impact resistance, corrosion resistance, electrical conductivity, thermal shock resistance and fire retardation, and UV protection. Thin films consisting of nanoparticles have a wide range of applications, such as nanoelectronics, magnetic storage devices, optical grating, and antireflective coating. For many of the nanoparticle-coating and thin-film-deposition applications, the nanoparticles have to be carried in the form of high-speed beams. This usually involves dispersing, deagglomerating, charging, and accelerating the nanoparticles.

Over the past few decades, researchers have been focusing on finding an efficient and reliable source of charged particles with a suitable charge-to-mass ratio for various applications. Methods of producing charged particles fall into several main categories, such as direct contact, induction, conduction, and charge injection. In practice, charged particles can be generated in a variety of ways; for example, from vapor condensation with electron injection, from ion nucleation, and from polarized surface condensation [1,2]. However, the use of electrostatic atomization offers a number of advantages

Received 9 March 2009; revision received 21 August 2009; accepted for publication 27 October 2009.

*Aerospace and Energetics Research Program, Box 352250.
†Professor, Aerospace and Energetics Research Program, Box 352250. Senior Member AIAA.

over other methods and has been investigated over the past few decades [4–17]. Use of electrostatic spraying techniques as a means for producing charged particles has evolved as a mature method in areas, such as low thrust level colloid thrusters, electrospray painting, semiconductor industry, medical research, bioengineering, and nanotechnology.

In a conventional electrospraying method, a slightly conductive electrolytic liquid is channeled through a capillary needle and emitted from a tip opening in the needle. At the same time, a strong electric field is applied at the tip opening of the needle, thereby causing an imbalance between the surface tension and the electrostatic force, due to the accumulation of charges on the surface of the liquid. If both the liquid flow rate and the electric field at the needle tip opening are maintained at proper levels, a liquid cone (commonly referred to as a Taylor cone) is formed at the needle tip along with a jet issuing forth from the cone's apex [5]. The Taylor cone, described by G. I. Taylor in 1964, is a stationary meniscus that forms in a liquid in the presence of an electric field [16]. The shape of the meniscus is determined by a balance of the electrostatic force and the liquid pressure and surface tension. The electrohydrostatic condition, as well as the surface charge density as a function of the local radius of curvature of the menisci, is determined by the liquid properties and the applied electric field. When the local electrostatic force at the tip of the cone exceeds the net liquid force, a jet emanates from the cone. As the jet travels further away from the Taylor cone, the jet eventually becomes unstable and breaks into a spray of charged particles. In this form, the spray of charged particles, or electrospray, is said to be in a cone-jet mode [6].

Despite the great successes of the cone-jet mode in producing charged particles, applications of this technology are still limited. Such relegation is mostly due to 1) the low liquid flow rate and 2) the relatively wide particle size and charge-to-mass ratio distribution. Inability to produce sufficient properly charged particles greatly limits the application of this technology in space propulsion, because it leads directly to low thrust level. In an attempt to overcome the low propellant flow rate, individual electrospray nozzles are integrated into an emitter array. However, it has been found that the integration of an emitter array at a high number density is technically challenging [12,13].

To improve the performance of electrostatic propulsion and nanotechnology applications, a new technology capable of producing nearly monodisperse, appropriately charged nanoparticles must be developed. To meet the performance requirements, this new method will have to meet the following criteria:

1) A high material processing rate (propellant flow rate) must be achieved.

2) A wide range of materials must be processed, from pure liquid to solid particle suspensions.

3) A high system reliability that allows continuous operation over a long duration is required.

4) A uniform particle size and appropriate charge-to-mass ratio must be maintained.

The research work described in this paper involves developing a new method of producing nearly monodisperse, appropriately charged electrospray at a high flow rate. The new method is based on the ultrasonically aided electrospray (UAE) concept [18], which uses charged capillary standing waves at the critical stable condition to produce charged particles. The UAE concept and the critical stable condition are described in the following sections; additional details are provided in [18,19].

II. Basic Principles of the Ultrasonically Aided Electrospray Concept

The UAE concept uses charged capillary standing waves at the critical stable condition to produce a high flux, nearly monodisperse electrospray. In this method, liquid is dispensed on the top surface of a diaphragm to form a thin liquid film; the diaphragm is vibrated by a piezoelectric transducer operating in frequencies ranging from 20 to several MHz to form capillary standing waves in the liquid film. The capillary standing waves in the liquid film have a wavelength on the order of micrometers or less. The vibration amplitude is controlled, such that the capillary standing waves maintain the critical stable condition (i.e., the threshold of atomization inception, at which surface tension and inertial forces balance at the wave crest of a capillary standing wave). A strong electric field is then applied to the capillary standing waves. Because of the charge accumulation, electrostatic pressure builds near the wave crests, causing an imbalance between the surface tension and the combined inertial and electrostatic forces. The introduction of electrostatic pressure on the liquid surface leads to an instability of the capillary standing waves, which produces a spray of fine-charged particles. Particle size depends on the vibration frequency, the applied electric field, and the liquid properties, such as surface tension, density, and viscosity. Particle sizes can range from the nanometer to micrometer scale. The particle size and charge-to-mass ratio can be precisely controlled by adjusting the operating parameters, such as the vibration frequency, vibration amplitude, the intensity of the applied electric field, and the liquid flow rate.

Figure 1 shows a sketch of the major components of a UAE system. The system consists of an ultrasonic nozzle powered by piezoelectric transducers, a liquid feed system, a HV power supply, and a conductive grid that serves as the extractor. The liquid feed system provides a controllable and stable liquid flow to the ultrasonic nozzle. The piezoelectric transducers in the ultrasonic nozzle are powered by a broadband function generator (not shown in the sketch) operating at the proper frequencies. The piezoelectric transducers convert the oscillating electrical signal to a mechanical vibration at the same frequency. Through a horn in the ultrasonic nozzle, the mechanical vibration of the piezoelectric transducers is transferred to the nozzle tip, also known as the atomization surface. A horn is only needed to amplify the vibration amplitude. The piezoelectric transducers can be designed to work over a wide range of frequencies, from several kHz up to the MHz range. In this work, frequencies ranging from 25 to 120 kHz are investigated. When the vibration frequency is high, direct contact between the piezoelectric transducers and the diaphragm is preferred, due to the simplicity and efficiency.

When liquid is fed to the ultrasonic nozzle and reaches the atomization surface at the nozzle tip, it forms a thin liquid film, due to the surface tension and wetting effects; the vibration of the atomization surface induces capillary standing waves in the liquid film. The HV power supply that connects to the nozzle tip and the extractor develops a strong electric field across the gap between the nozzle tip and the extractor. The electric field causes charge accumulation at the tip of the capillary standing waves.

The UAE concept uses charged capillary standing waves to produce monodisperse uniformly charged particles. Capillary standing waves at the critical stable condition form a rectangular grid pattern on the surface of the liquid, with regularly alternating crests and troughs extending in both directions. Atomization inception does not occur until a sufficient electric field is applied to the capillary standing waves. This process is distinguished from the atomization process, driven purely by vibration, in which the rectangular grid wave pattern becomes disordered at the inception of atomization [20]. The disorder increases after atomization takes place, and the particle

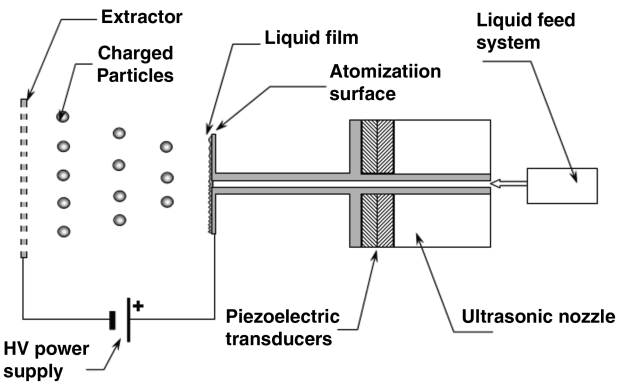

Fig. 1 Diagram of a UAE system.

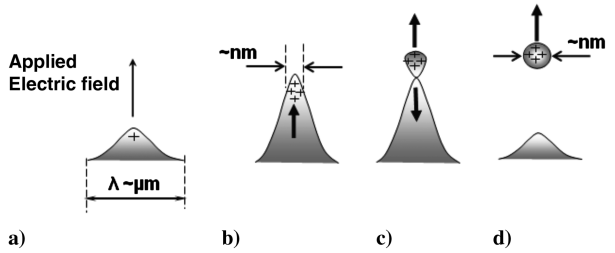

Fig. 2 A schematic representation of the evolution process of a charged capillary standing wave at critical stable condition.

formation positions are randomly distributed across the film, in contrast to the well-maintained organized grid pattern before the inception of atomization.

Figure 2 schematically shows the different stages of particle formation from a charged capillary standing wave at the critical stable condition. The bold arrows indicate the direction of the liquid motion in the capillary standing wave. When the capillary standing waves in the liquid film reach the critical stable condition, the introduction of the electric field causes charge accumulation at the wave tip, as shown in Fig. 2a. As the capillary standing wave absorbs more vibrational energy and grows in amplitude, the wave tip becomes sharper, and the surface charge density becomes higher, as shown in Fig. 2b. In Fig. 2c, the capillary standing wave reaches its maximum amplitude. If the combined electrostatic pressure and inertial forces exceed the surface tension when the wave starts to recede, the liquid near the wave tip detaches from the wave, and a charged particle is emitted, as shown in Fig. 2d. In such a process, the introduction of an electric field triggers the inception of atomization. The electrospray, consisting of charged particles, is positively or negatively charged, depending the polarity of the applied voltage. The system can be operated with an oscillating polarity, as an AC circuit, to emit a time-averaged neutral electrospray.

The method of producing charged particles using standing capillary waves is similar to the method based on the cone-jet mode, except that the nozzle-supported stable Taylor cones are replaced by the capillary standing waves. Compared with the cone-jet mode, this method has the following advantages:

1) The critical condition of the capillary waves makes it easier for charged particles to form and detach from the tip of the wave.

2) The critical condition of the capillary waves also reduces the intensity of the electric field required to extract charged particles from the waves, and ion evaporation directly from the liquid meniscus is unlikely to take place; therefore, a more uniform charge-to-mass ratio distribution in the electrospray is expected.

3) The extremely large concentration of capillary standing waves greatly increases the flux of the electrospray. Considering that a typical wavelength of interest is around 10 μm or less, a minimum of 1 million capillary standing waves per cm^2 of atomization surface area is expected. Each capillary standing wave is equivalent to an emitter in the regular cone-jet mode for producing electrospray.

III. Theoretical Analysis

A. Formation of a Charged Particle at the Tip of a Charged Capillary Standing Wave

A charged capillary standing wave at the critical stable condition differs fundamentally from a stable Taylor cone in the cone-jet mode because of the dynamical characteristics involved in capillary standing waves. However, there are some similarities between these two phenomena. For most of the conductive liquids of interest, the charge relaxation time is much shorter than the vibration period of the capillary standing waves [4]. The charge relaxation time characterizes the time required for free charges to reequilibrate in response to an externally applied electric field. This implies that charge accumulation at the tip of a capillary standing wave occurs in a time much less than the time for the standing wave to develop. Therefore, a Taylor cone develops at the tip of the wave crest when the wave reaches its maximum amplitude. The electric field normal to the surface near the wave crest of a capillary standing wave at its maximum amplitude is assumed to be identical to that of a stable Taylor cone without a jet. The electrostatic pressure applied to the surface of the capillary standing wave is calculated, and a linear stability analysis is performed on a charged capillary standing wave.

A standing wave at its highest amplitude, with a Taylor cone on the wave tip (as shown in Fig. 3) is investigated. The electric field reaches the maximum near the tip of the Taylor cone where the liquid meniscus takes a partial spherical shape with a local radius of R_o. The electrostatic pressure on the surface of the cone, due to the surface charge, is [21]

$$P_e = \frac{\varepsilon_o E^2}{2} \tag{1}$$

Because the capillary standing waves are formed on a free liquid surface, the liquid pressure is equal to the ambient pressure, or zero in the case of a capillary standing wave in a vacuum. In either case, the liquid pressure has no effect on the equilibrium of the surface pressure. The maximum electric field is reached when the electrostatic pressure is balanced by the pressure due to surface tension force, which is given by

$$P_{\text{st}} = \frac{2\sigma}{R} \tag{2}$$

The electric field normal to the liquid surface at the tip of the cone is determined by combining Eqs. (1) and (2):

$$E = 2\left(\frac{\sigma}{\varepsilon_o R_o}\right)^{1/2} \tag{3}$$

The electric field has a constant value on the spherical portion of the meniscus surface. The transition from the spherical surface to the conical surface occurs at $r = R_o \cos\alpha$. The dependence of the particle size and charge-to-mass ratio on the electric field is determined by expressing all variables in terms of E. From Eq. (3), the local radius R_o is

$$R_o = \frac{4\sigma}{\varepsilon_o E^2} \tag{4}$$

From the geometric relationship shown in Fig. 3,

$$r_o = R_o \cos\alpha = \frac{4\sigma}{\varepsilon_o E^2}\cos\alpha \tag{5}$$

Because, on a partial spherical meniscus (shaded area in Fig. 3) near the tip of a fully charged Taylor cone, $r < r_o$, the electrostatic pressure equals the surface tension force. As a result, when an inertial force is added to the meniscus at equilibrium (such as, when the standing wave starts to recede), a jet issues from the cone's apex. However, unlike the continuous liquid jet found in the cone-jet mode, such a jet is unstable and is not sustained. The vibration of the wave introduces perturbations that cause varicose breakup of the jet. The jet eventually degenerates into a single particle, emitting from the tip of the wave before the jet is fully developed. Most of the charge

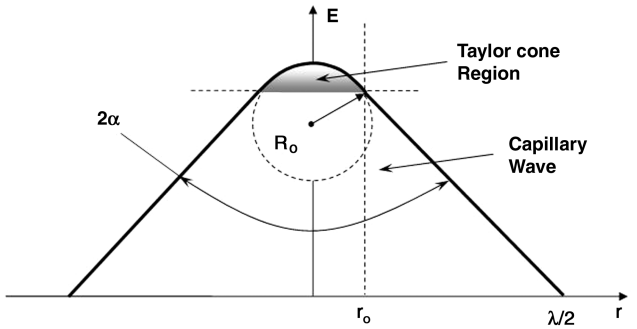

Fig. 3 Capillary standing wave with a transiently stable Taylor cone at the crest.

accumulates in the jet tip as it develops, leaving the rest of the cone essentially uncharged. It is possible for the jet to degenerate into multiple particles, but this is not observed in the experiments presented here. This process differs slightly from the simplified description of Fig. 2, in which the process is described as a particle ejecting from the crest of a charged capillary standing wave without the jet development.

The size of charged particles emitted from a degenerating charged capillary standing wave is estimated from the diameter of the jet. Theoretically, the jet diameter can be any value less than $2r_o$. As the wave decays and the jet elongates, the jet diameter must approach $2R_o$ to maintain the equilibrium condition in the liquid meniscus at the tip of the jet, otherwise the electric field at the jet tip will exceed the initial electric field.

Assuming a jet diameter of $2R_o$, the final particle size is determined from the neck location in the cylindrical jet, as shown in Fig. 4. When the capillary wave starts to recede, the partial spherical surface at the wave crest starts to stretch into a cylindrical jet. The jet eventually breaks up into discrete particles. The neck location is determined using Rayleigh's capillary breakup theory for a cylindrical jet, which is based on the breakup of free surface flows controlled by surface tension [22]. The jet breaks up into segments with a maximum length of $9R_o$. Shorter segments are possible for small amplitudes (less than $9R_o$) of the standing waves. However, for this application, R_o is usually several orders of magnitude less than the wave amplitude. If nonlinear effects and the influence of the surface charge on the jet stability are neglected, the volume of the particles produced by the jet breakup is equal to the volume of a cylindrical liquid column, which is approximately

$$V = \pi R_o^2 \Lambda = 9\pi R_o^3 \tag{7}$$

The corresponding particle radius r_d is given by

$$\frac{4}{3}\pi r_d^3 = 9\pi R_o^3 \tag{8}$$

which yields $r_d = 1.89R_o$. When expressed in terms of the applied electric field E, by substituting into Eq. (4), the particle radius is given by

$$r_d = \frac{7.56\sigma}{\varepsilon_o E^2} \tag{9}$$

and the charge-to-mass ratio for fully charged particles is given by Rayleigh's stability criterion, applied to the liquid meniscus of the cone tip [17]:

$$\frac{q}{m} = \frac{6(\sigma\varepsilon_o)^{1/2}}{\rho r_d^{3/2}} = \frac{0.29\varepsilon_o^2 E^3}{\rho\sigma} \tag{10}$$

This criterion assumes that the particle is fully charged before it detaches from the wave. This assumption is valid, provided the atomization is dominated by electrostatic pressure. Experimental results based on the cone-jet mode have also indicated that particles released from a jet are nearly fully charged [7]. A more accurate prediction of the surface charge density requires a complete solution of the liquid flow and charge convection within the jet region [6].

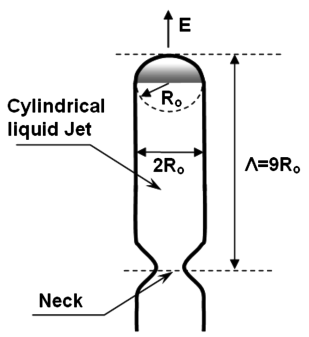

Fig. 4 Evolution of a cylindrical jet from a transiently stable Taylor cone.

The maximum current carried by the charged particles emitted from an individual standing wave can also be obtained:

$$I = \frac{q\omega}{2\pi} = \frac{\omega}{2\pi}\frac{6(\sigma\varepsilon_o)^{1/2}}{\rho r_d^{3/2}} m = 83.14\frac{\omega\sigma^2}{\varepsilon_o E^3} \tag{11}$$

The maximum current density that can be supported by the capillary standing waves in a liquid film is then

$$j = \frac{I}{\lambda^2} = 83.14\frac{\omega\sigma^2}{\varepsilon_o \lambda^2 E^3} \tag{12}$$

In this analysis, an implicit assumption is that the capillary standing waves are small enough for each to support a Taylor cone. The local radius of the liquid meniscus R at the tip of an uncharged capillary standing wave must be comparable with the radius of the partial spherical surface R_o at the tip of the Taylor cone. If R is much larger than R_o, the local curvature of the wave surface is too small to cause a local charge concentration when the electric field is applied, Taylor cones are not produced by the capillary standing waves, and the charging mechanism described is not established. Even though charged particles can still be produced by vibration only, the size of the particle is controlled by vibration-induced atomization and is not significantly affected by the applied electric field.

It should be noted that the emission of charged particles from charged capillary standing waves involves strongly nonlinear effects, especially when the vibration power is high and the organized and generally orthogonal standing wave pattern found before the atomization inception becomes disordered during the atomization. These nonlinear effects adversely affect the spray particle size and charge-to-mass ratio. The vibration power should be controlled, such that the capillary waves maintain the rectangular wave pattern; the applied electric field is then adjusted to achieve the inception of atomization and control the spray particle size and charge-to-mass ratio. Maintaining an organized wave pattern reduces the nonlinear effects and keeps the size and charge-to-mass ratio more uniform.

B. Analysis of Particle Size, Charge-to-Mass Ratio, and Velocity, Based on Global Experimental Measurements

The spray particle size, velocity, and charge-to-mass ratio can be measured in a number of different approaches. Mie scattering provides accurate particle size distributions [23]. Retarding potential analyzers, time-of-flight (TOF) measurements, and quadrupole mass spectrometers have provided a measure of the charge-to-mass ratio of charged species emitted from Taylor cones [24]. TOF also provides the particle velocity. This section derives relations between spray particle size, charge-to-mass ratio, and velocity and experimentally measured global parameters, such as the total spray current, the liquid flow rate, and the accelerating voltage. The approach is valid only if the following assumptions hold:

1) All particles released from the charged capillary waves are fully charged [i.e., the spray particle charge-to-mass ratio is given by Eq. (10)].

2) The current carried by the electrospray is determined by the Child–Langmuir law:

$$j = \frac{4\varepsilon_o}{9}\left(\frac{2q}{m}\right)^{1/2}\frac{\mathbf{V}^{3/2}}{d^2} \tag{13}$$

If the total spray current and liquid flow rate are known, the average charge-to-mass ratio $\langle q/m\rangle$ of the spray particles is given by

$$\left\langle\frac{q}{m}\right\rangle = \frac{I}{\rho Q} \tag{14}$$

where $\langle\ldots\rangle$ indicates an average value. Q is the volume flow rate of the liquid. Based on the assumption that the spray particles are fully charged, the Rayleigh instability criteria in Eq. (10) can then be used to calculate the average radius of the particle:

$$\langle R\rangle = \left(\frac{36\sigma\varepsilon_o}{\rho^2(q/m)^2}\right)^{1/3} \tag{15}$$

The average charge-to-mass ratio can also be calculated if the current carried by the electrospray is space charge limited. From Eq. (13), the particle charge-to-mass ratio can be expressed in terms of current density, applied voltage, and grid distance, as

$$\frac{q}{m} = \frac{81}{32}\frac{j^2 d^4}{\varepsilon_o^2 \mathbf{V}^3} \tag{16}$$

The current density is

$$j = \frac{I}{S} \tag{17}$$

where S is the effective atomization surface area. The particle radius is given by Eq. (15), expressed in terms of I and S:

$$\langle R\rangle = \frac{16\mathbf{V}^2}{9}\left(\frac{\sigma\varepsilon_o^5 S^4}{\rho^2 I^4 d^8}\right)^{1/3} \tag{18}$$

Once the average particle size is obtained, the surface charge emission limit

$$\frac{q}{m} = \frac{3\varepsilon_o E_s}{\rho r} \tag{19}$$

is then used to verify that a fully charged particle of the size given by Eqs. (15) or (18) is stable (i.e., such a particle can exist without emitting ions from its charged surface). E_s is the threshold electric field, above which direct ion emission from a charged particle surface occurs.

Figure 5 plots Eq. (18) for a 2 kV applied voltage and a 10 mm grid distance. The working liquid is assumed to be salt water at 25°C, with salinity of 2% and electric conductivity of 33 mS/cm. The atomization surface is assumed to be a circular area with a 1 mm diameter. Figure 5 shows that, for fully charged spray particles, the particle size is inversely related to the spray current (i.e., higher current produces smaller spray particles with higher charge-to-mass ratios).

The average spray particle velocity can be determined from global parameters, such as total spray current, liquid volume flow rate, and the applied voltage. At a steady operating condition, energy conservation gives

$$\tfrac{1}{2}(\rho Q)u^2 = \mathbf{V}I \tag{20}$$

which yields

$$u = \left(\frac{2\mathbf{V}I}{\rho Q}\right)^{1/2} \tag{21}$$

Equation (21) provides a convenient way of finding the average spray particle velocity in an electrospray. However, a wide charge-to-mass ratio distribution produces a nonuniform velocity. The average spray particle velocity obtained using global quantities provides limited information in describing the velocity distribution of the electrospray. In that case, a direct particle velocity measurement method should be used.

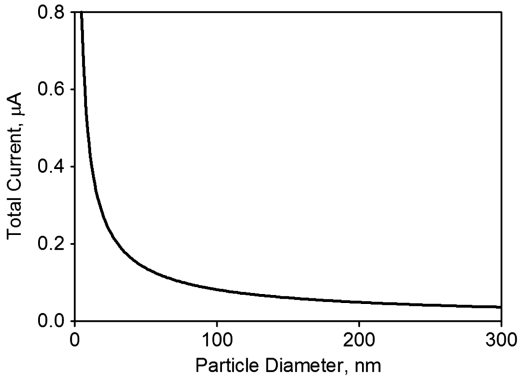

Fig. 5 Dependence of particle diameter on the total spray current. The curve is derived from Eq. (18).

IV. Experimental Setup

An experimental UAE system requires the solution to a few technical problems. First, a uniform thin liquid film covering a large surface area on a surface vibrating at a high frequency must be maintained. In addition, the vibration amplitude has to be controlled, such that the capillary standing waves are maintained at the critical stable condition. Finally, the capillary standing waves need to be charged properly, such that the charged particles can be produced with narrow size and charge-to-mass ratio distributions. Reflected in the hardware selection and design, a successful experimental UAE system requires 1) a means of dispensing a liquid in a stable and controllable manner on the surface of a diaphragm to form a uniform thin liquid film, 2) a large vibrating surface driven by high frequency piezoelectric transducers, for which the vibration power output can be controlled accurately over a wide range, such that the required critical stable condition of the capillary standing waves can be achieved, and 3) a means of charging the capillary standing waves to the required potential without affecting the performance of the electrically sensitive piezoelectric transducers.

To maintain a stable and accurate flow rate, as stated in requirement 1), an accurate digitally controlled syringe pump (Sono-Tek model 997) is used. The pump can be programmed to deliver a constant flow rate. The flow rate range is 0.001–30 ml/min, and the flow rate stability is ±1%. An ultrasonic nozzle (Sono-Tek model 8700-120) is used to generate capillary standing waves in a thin liquid film. The operating frequency is 120 kHz. This nozzle can operate over a wide range of input power, such that requirement 2) is satisfied. Once the capillary standing waves are established in the thin liquid film over the large surface area, charging the waves properly is accomplished by applying an electric field using a HV power supply. The EMCO model 4300 HV power supply used in this system is continuously adjustable over a 0–30 kV range. The maximum output current for this HV power supply is 0.33 mA.

Figure 6 shows a schematic cutaway overview of the experimental system setup. The ultrasonic nozzle and the extractor are mounted on Teflon plates for electrical isolation and are placed in a bell jar, which eliminates the effects on the air current on the resultant electrospray. The bell jar and the vacuum system also enable investigations in the

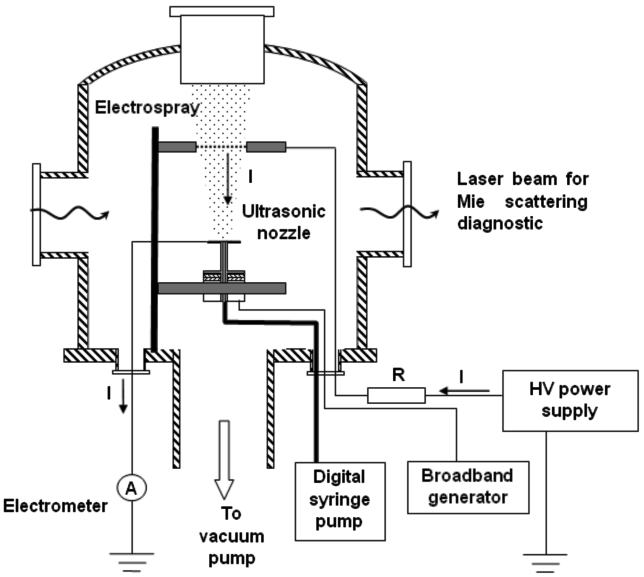

Fig. 6 Schematic cutaway view of the experimental UAE system. The experimental system is implemented with a vacuum bell jar, providing the capabilities for studies in a vacuum, and it eliminates air currents.

vacuum. In this system design, the extractor is charged to positive potential by the HV power supply, and the ultrasonic nozzle is grounded to avoid the application of HV to the piezoelectric transducers. An electrometer is connected to the circuit between the ultrasonic nozzle and the ground to measure the spray current. Only the ultrasonic nozzle and the HV power supply are grounded in this UAE system, to avoid multiple current paths. This ensures that all the spray current flows through the electrometer.

In this study, the spray particle size and size distribution are measured using both a Mie scattering diagnostic and witness plates examined with an atomic force microscope (AFM). Mie scattering for particle size and size distribution measurement entails directing a laser through the electrospray, measuring the angular scattering pattern that is produced, and then using the Mie scattering theory to infer the particle size distribution [23].

Glass witness plates are exposed to the electrospray to collect particles. The exposure is limited to avoid overlapping particles on a witness plate. The witness plates are examined with an AFM. The AFM is a high-resolution type of scanning probe microscope, which has a resolution of fractions of a nanometer.

Water is a commonly used solvent to create nanoparticle suspension. In this work, room-temperature (21°C) tap water is used for the majority of the studies, in an atmospheric pressure environment. Tap water is an acceptable medium for these experiments, because it has a finite electrical conductivity and has dissolved minerals that facilitate identifying particle edges. Zinc oxide (ZnO) nanoparticle suspension in water with a volume concentration of 4.2% is used in the studies using witness plates, in which the ZnO nanoparticles have an average diameter of 30 nm. It should be noted that ZnO nanoparticles are used here only to facilitate droplet size measurement. The ZnO nanoparticles used in the experiments should be differentiated from the electrospray droplets (referred to as charged particles in this paper) that are produced using the experimental UAE system. Although the ultimate goal is to produce charged nanoparticles using the UAE technology, this goal has not been demonstrated in the experiments described in this paper.

Water cannot be used in a vacuum due to the high vapor pressure. When water is introduced into a vacuum, it evaporates rapidly and freezes, which makes it unable to form a thin liquid film. For vacuum testing, formamide solutions and tributyl phosphate have lower vapor pressures and are used for experiments in a vacuum. These results are not reported here.

Operating parameters of the UAE system include the liquid flow rate, the applied voltage, the grid distance, the nozzle vibration power, and the vibration frequency (which is specific to each nozzle design). Nozzles with different frequencies are used in the study, but only the results from the 120 kHz nozzle are reported here. The electrical conductivity of the liquid is also considered as a parameter that defines the experimental condition. However, due to the difficulties of controlling the electric conductivity of the liquid accurately, a quantified study is not conducted. The effects of these operating parameters on the spray current, spray particle size, and charge-to-mass ratio are investigated. Some of the experimental results are discussed in the following section.

V. Experimental Results and Discussion

The objective of the experimental study is to gain a basic understanding of the UAE method for producing monodisperse charged particles, specifically: 1) experimental verification of the critical stable condition of charged standing waves, and 2) characterization of the electrospray produced by charged capillary standing waves at such a condition. The effects of different operating parameters on the production of electrospray, using charged capillary standing waves, are also investigated.

A. Experimental Verification of the Critical Stable Condition of Capillary Standing Waves

The critical stable condition is determined by the vibration amplitude and frequency for a given liquid. It is maintained by adjusting the vibration amplitude of the capillary standing waves, such that the waves are marginally stable and no particles are ejected from the capillary standing waves without an applied electric field. After the electric field is applied, the accumulation of free charges introduces an electrostatic pressure on the surface of the marginally stable wave, which leads to particle emission from the capillary standing waves.

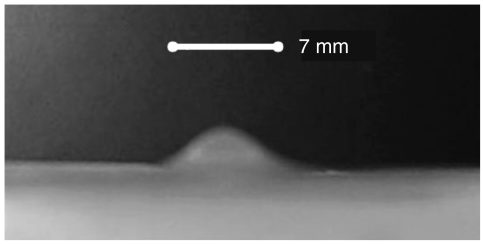

Fig. 7 A standing wave at its maximum amplitude is produced without applied voltage.

To study the critical stable condition, a large-scale experiment is designed to produce a single-period standing wave that is clearly visible. A piezoelectric transducer is placed 90 mm underwater in a small container to establish a standing wave on the water surface at a frequency of approximately 1 Hz. The standing wave is set with the fundamental mode with a half-wavelength of approximately 7 mm. An extractor grid is placed above the standing wave, and the distance between the extractor and the wave crest is adjustable. The extractor connects to a HV power supply to establish an electric field between the standing wave and the extractor.

Figure 7 shows the wave at its maximum amplitude without an applied voltage. The vibration amplitude is adjusted, such that the wave is at a marginally stable condition and no particles are produced. Figure 8 shows images from a video sequence, showing the evolution of the standing wave after an electric field is applied. The extractor is above the liquid surface, with an adjustable grid distance, and 8 kV are applied. Figure 8a shows the initial development of a charged standing wave. The image in Fig. 8b indicates that when the charged standing wave reaches its maximum amplitude, the electric field causes the liquid meniscus at the wave crest to develop a conical shape, similar to the liquid meniscus at the electrohydrostatic equilibrium condition in the cone-jet mode. Comparing Fig. 8b with the uncharged wave surface, shown in Fig. 7,

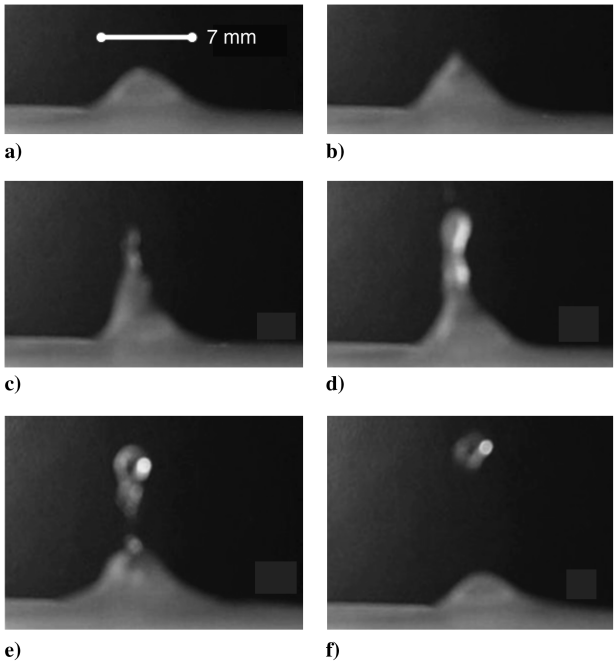

Fig. 8 Evolution of a charged standing wave at the critical stable condition with a 640 V/mm electric field applied. Time between frames is 60 ms.

the charged standing wave has a sharper wave tip and a smaller radius of curvature at the apex of the tip. As the wave continues developing, a jet issues from the apex of the wave tip and elongates, as shown in Fig. 8c. In Fig. 8d, as the standing wave starts to recede, the jet develops a varicose instability and begins to form necks. Figure 8e shows that the wave neck continues to grow and eventually pinches off the jet, and a charged particle is released from the wave. In Fig. 8f, the charged particle is completely detached from the degenerating standing wave and accelerates toward the extractor (not in the field of view of Fig. 8).

Even though the experimental conditions are carefully maintained at a repeatable status, the size of the droplets released from the tip of the wave changes dramatically from time to time. The wave breakup mechanism varies from time to time. Sometimes, the jet protrudes a long distance, and sometimes the jet is barely visible. Even when a jet forms, it breaks up before reaching a length of $9R_o$, as predicted analytically. This behavior is conjectured to be caused by the large perturbations from the vibration of the standing waves, which lead to premature instability of the jet before it reaches the full length predicted by Rayleigh's capillary breakup theory. The simplified critically stable condition for linear stability analysis is useful for describing the fundamental mechanism for the wave breakup process, but it misses some of the details and provides only an approximate description.

To quantify the effect of the applied electric field on the standing wave and emission of charged particles, the onset voltage (the minimum applied voltage required to trigger the inception of atomization for a previously stable standing wave) is measured at different grid distances. Figure 9 shows the dependence of the onset voltage (the minimum voltage required for electrostatic atomization in a previously stable standing wave) on the grid distance for the standing wave at three different vibration amplitudes: 2.0, 2.5, and 3.0 mm. The different wave amplitudes are achieved by adjusting the operating voltage of the piezoelectric transducer. The standing wave is at a marginally stable condition when the wave amplitude is 3.0 mm. The data in Fig. 9 show that the dependence of the onset voltage on the grid distance is a linear relationship for each wave amplitude, indicating that the corresponding electric field is approximately a constant. The electric field is calculated, based on the onset voltage and the grid distance. For the 2.0 mm wave amplitude, the calculated average applied electric field is 914 V/mm, with a standard deviation of 42 V/mm. For the 2.5 mm wave amplitude, the corresponding average applied electric field is 735 V/mm, with a standard deviation of 8 V/mm. For the 3.0 mm wave amplitude, the corresponding average applied electric field is 640 V/mm, with a standard deviation of 6 V/mm.

Results shown in Fig. 9 indicate that, for a standing wave at a given vibration frequency and amplitude, the stability of the wave is mainly determined by the applied electric field. The onset electric field decreases when the wave amplitude increases. Waves at the marginally stable condition have the lowest onset electric field. Furthermore, the linear fit to compute the electric field required for particle emission has a smaller standard deviation for the lower onset electric field (640 ± 6 V/mm) than for the higher onset electric fields (735 ± 8 V/mm and 914 ± 42 V/mm), indicating that the release of charged particles from waves at the critical stable condition is more consistent than from more stable waves. The deviation of the data points away from the linear fit is evident in Fig. 9.

Evidence of the critical stable condition is also observed in the experiments with the capillary standing waves. The 120 kHz nozzle generates a water electrospray at a vibration power of 0.3 W and a flow rate of 5 ml/hr when a sufficient electric field is applied. For a grid distance of 35 mm, the onset voltage required to maintain a steady atomization is approximately 9 kV, or 257 V/mm. When the applied voltage is below this value, atomization is not sustained and liquid accumulates on the atomization surface at the nozzle tip. This behavior is consistent with the electric field extracting charged particles from standing waves at the critical stable condition to produce the electrospray.

When a steady atomization is maintained using the 120 kHz nozzle, it is observed that the current carried by the spray varies with the nozzle vibration power and the applied electric field. Figure 10 shows the spray current dependence on the nozzle power at four different applied voltages (4, 5, 6, and 7 kV) with the extractor grid located at 10 mm, with corresponding accelerating electric fields of 400, 500, 600, and 700 V/mm. The working liquid is tap water at atmospheric pressure, and the liquid flow rate is 15 ml/hr. Each set of data shows that the spray current reaches the maximum when the nozzle power is 0.7 W; above this power level, the spray current decreases as the nozzle power increases. Data in Fig. 10 also show that when the nozzle power is less than 1 W, there is a significant spray current increase when the applied voltage is increased. As the nozzle power approaches 4.5 W, the spray currents for the four applied voltages converge to a substantially lower level.

The spray current increases abruptly when the applied voltage exceeds 5 kV, as shown in Fig. 10. When the applied voltage is below 5 kV, the spray current is maintained at a relatively low level, with a peak value of less than 42 nA. Below this applied voltage level, the spray current increases at a lower rate with the applied voltage. For example, when the applied voltage is increased from 4 to 5 kV, the peak spray current rises from 33 to 42 nA, a 27% increase. However, when the applied voltage is increased from 5 to 6 kV, the peak spray current rises from 42 to 64 nA, a 52% increase. The spray current is observed to maintain the higher rate for larger applied voltages. When the applied voltage is increased from 6 to 7 kV, the corresponding peak spray current increases from 64 to 93 nA. This behavior of the spray current is consistent with the previously discussed critical stable condition of the capillary standing waves. When the applied voltage is below the threshold value, the effect of the electric field on the stability of a capillary standing wave is insignificant, and the atomization is dominated by the vibration. The spray particle size and the charge-to-mass ratio are primarily determined by the vibration-induced atomization and the Rayleigh stability criteria. As the applied voltage is increased, the electric field reaches a threshold value, at which the effect of the electric field becomes and dominates the atomization.

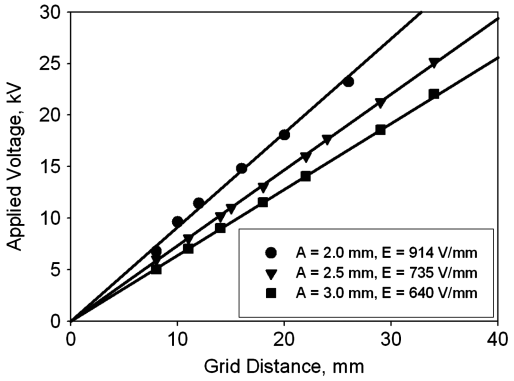

Fig. 9 Dependence of onset voltage on the grid distance for a charged standing wave. (Applied voltages are measured with ±50 V accuracy.)

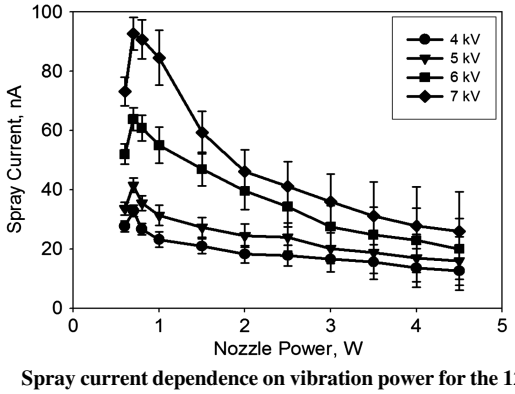

Fig. 10 Spray current dependence on vibration power for the 120 kHz nozzle at four different applied voltages and corresponding electric field values of 400, 500, 600, and 700 V/mm.

As discussed earlier, the critical stable condition is a marginally stable condition. Such a condition exists only when the nozzle vibration power is low. For the 120 kHz nozzle used in this study, this power level appears to be between 0.3 and 1.0 W, depending on the liquid flow rate. Figure 10 shows that when the nozzle power is increased above 0.7 W, the spray current decreases for all applied voltage levels, with a larger decrease for the 6 and 7 kV conditions. Higher nozzle power destroys the critical stable condition and reduces the influence of the applied electric field. Spray particles are then produced from insufficiently charged capillary standing waves, and the corresponding spray charge-to-mass ratio and spray current are reduced. When the nozzle vibration power is high, the atomization becomes vibration dominant and the spray current becomes less dependent on the applied voltage. Therefore, all the curves converge to a low spray current value when the nozzle power is high.

Based on these experimental results, two distinct operating regimes of the UAE system can be identified. In the vibration-dominant regime, the electrostatic pressure due to the applied electric field is too weak to affect the stability of the capillary standing wave and does not significantly affect the spray. In the electric-field-dominant regime, electrostatic pressure strongly affects the stability of the capillary standing waves, reduces the spray particle size, and improves the spray particle size uniformity.

The two operating regimes are primarily determined by the nozzle vibration frequency and the applied electric field. However, other parameters, such as the liquid properties (viscosity, surface tension, etc.), the liquid flow rate, and the wave vibration amplitude, are also relevant. Liquids with high viscosity or surface tension coefficient require a larger applied electric field to operate in the electric-field-dominant regime.

Vibration-dominant atomization does not produce fully charged particles. The electrospray is produced from insufficiently charged waves, instead of the fully charged liquid meniscus in waves at the critical stable condition. Even though the spray particles can still be charged, however, the particle sizes and the charge-to-mass ratio vary more than those of an electrospray produced by capillary standing waves at the critical stable condition. The capillary standing waves are not maintained at the critical stable condition in the vibration-dominant regime. However, the standing waves must have a sufficiently high amplitude, such that the radius of curvature of the liquid meniscus at the wave crest is small enough to allow a significant charge accumulation. Waves with insufficient vibration energy can maintain a stable condition and fail to produce an electrospray even with the electric field applied.

Not all capillary waves are likely to be maintained at the critical stable condition at all times. At any give time, possibly only a portion of the capillary waves are at a condition close to the critical stable condition, or for a particular capillary standing wave, it may only maintain the critical stable condition for a fraction of the time during its life span.

B. Characterization of Electrospray Particles Produced at the Critical Stable Condition

The electrospray particles are characterized by both a Mie scattering diagnostic and witness plates examined with an AFM. Figure 11 shows the electrospray particle size distribution, for the 120 kHz nozzle, measured with the Mie scattering diagnostic. The experiment is conducted at atmospheric pressure, using tap water as the working liquid. The liquid flow rate is 15 ml/hr. The nozzle frequency is 120 kHz, and the vibration power is 0.7 W, which is the lowest level required to produce spray at this flow rate. This ensures that the capillary standing waves are maintained at a state that is close to the critical stable condition when the waves are charged. The extractor grid is located 20 mm from the atomization surface, and the applied voltage is varied with values of 0, 6, 8, 12, and 16 kV, with corresponding accelerating electric fields of 0, 300, 400, 600, and 800 V/mm.

The Mie scattering data shown in Fig. 11 and Table 1 demonstrate a reduction in spray particle size and an improvement of the spray particle size uniformity with increasing of the applied electric field, which is indicative of operating in the electric-field-dominant regime. The dotted curve shows the particle size distribution when the atomization is solely driven by vibration. The other curves are for the same conditions but with different applied voltages. The size distribution curves demonstrate that both electrospray particle size and variation [full-width half-maximum (FWHM)] of the size distribution curves decrease as the applied electric field increases. The mean particle diameter decreases from 41.4 μm for the uncharged condition to 22.9 μm for an 800 V/mm accelerating electric field (16 kV applied voltage). The corresponding FWHM of the size distribution curve decreases from 50.9 to 10.7 μm. These results show that, as the electric field increases, the electrospray production is affected more strongly by the electric field and less by the vibration energy. The observed behavior is consistent with the theoretical understanding of the effect of the applied electric field on both the size and size distribution of spray particles [i.e., larger electric fields produce charged particles of smaller size, as shown by Eq. (9)], with improved size uniformity, which is the result of reduced random vibrational effects on the atomization. Table 1 summarizes the characteristics of the particle size distribution corresponding to each applied electric field value.

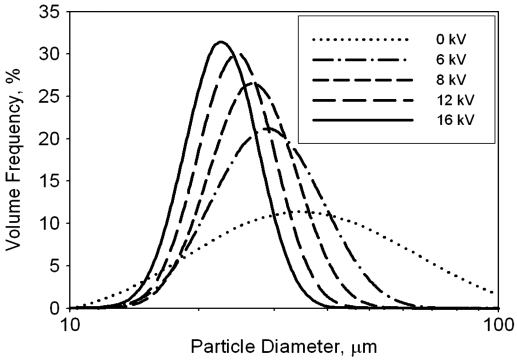

Fig. 11 Particle size distribution measured with the Mie scattering diagnostic for different applied voltages and corresponding electric fields of 0, 300, 400, 600, and 800 V/mm.

Witness plates examined with an AFM are also used to measure the electrospray droplet size. (Hereafter, the term droplet is used for the spray particles to distinguish them from the ZnO nanoparticles that form the spray particles together with the liquid solvent.) ZnO nanoparticles with an average primary size of 30 nm are dispersed in tap water to create a nanoparticle suspension. Concentration of ZnO nanoparticles in the suspension is 4.2% by volume. The nanoparticle suspension is then deposited on a witness plate (flat glass slide) in the form of electrospray, using the experimental UAE system. The exposure of the witness plates to the electrospray is limited to avoid overlapping droplets. When the spray droplets strike the glass slide, each droplet forms discrete, thin liquid films. The solvent (in this case, water) evaporates, leaving a thin film of dry nanoparticles on the glass slide.

The thin films of ZnO nanoparticles on the glass slides are examined with an AFM. The thickness and size of the nanoparticle thin films are measured. Figure 12 shows an optical image of a nanoparticle film deposited on a glass slide, each of the thin films is created by a single droplet in the electrospray. The optical photographs are taken with an AFM. The applied voltage is 2.9 kV and the grid distance is 10 mm, giving a 290 V/mm accelerating electric

Table 1 Summary of particle size distribution

V, kV	E, V/mm	$\langle R \rangle$, μm	FWHM, μm
0	0	41.4	50.9
6	300	30.0	20.5
8	400	27.3	15.3
12	600	24.9	12.1
16	800	22.9	10.7

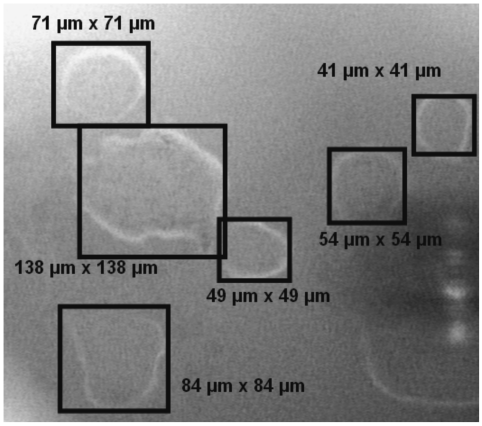

Fig. 12 ZnO nanoparticle thin films deposited on a glass slide witness plate.

field. The liquid flow rate is 15 ml/hr. The 120 kHz nozzle operating at 0.8 W is used to produce the electrospray. The nanoparticle thin films are measured and processed statistically. For this operating condition, 24 thin nanoparticle film samples are examined. The films are approximately round with diameters ranging from 30 to approximately 140 μm. Accuracy of size measurement is ± 2 μm. The average diameter of the thin film is 72 μm, and the standard deviation is 25 μm.

Figure 13 shows the AFM image of a nanoparticle film created by a single droplet in the electrospray. The dark background is the flat surface of the glass slide. The film thickness is measured along different chords through the nanoparticle film, as shown in Fig. 13b, to determine the average thickness. The image in Fig. 13 shows a thick rim surrounding each droplet, which, according to the AFM image, contains material that is different from ZnO nanoparticles in the inner area of the film. It is possibly dust or segregated minerals dissolved in tap water. In the nanoparticle thin film area measurement, the rim is excluded, and only the inner area of the nanoparticle film is considered. Data in Fig. 13b show an average film thickness of 46 nm.

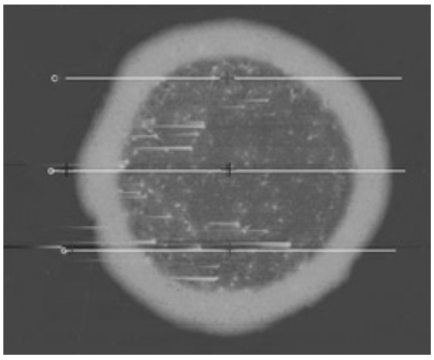

a)

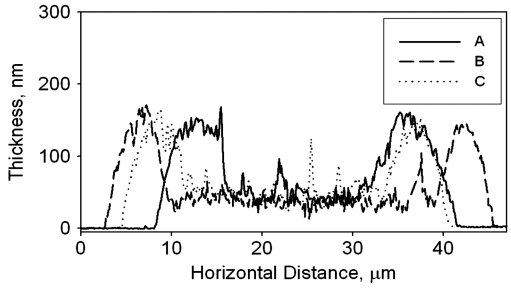

b)

Fig. 13 Sample AFM results for one of the thin films (not shown in Fig. 12): a) AFM image of a thin nanoparticle film; and b) thickness of the nanoparticle thin film along three different chords, indicated by the white horizontal lines shown in a) [A, B, and C denote the top, middle, and bottom lines in a)].

The average thickness of the nanoparticle film is used to calculate the amount of dry nanoparticles in the film. This information is then used to calculate the volume of the dry nanoparticles V_{particle} in a single droplet. If the nanoparticle volume concentration in the original suspension x is known, the volume of the original droplet V_{droplet} striking the witness plate can be determined:

$$V_{\text{droplet}} = \frac{V_{\text{particle}}}{x} \tag{22}$$

The droplet size is computed from the volume V_{droplet}, assuming a spherical droplet. For the conditions described in Fig. 12, the average film thickness is 46 nm and the average thin film diameter is 72 μm. The corresponding average droplet diameter, according to Eq. (22), is 20 μm, and the associated standard deviation is 5 μm, corresponding to a FWHM of 11 μm. Figure 14 shows the experimental data that are fit with a Gaussian distribution, with a 20 μm average droplet size and a FWHM of 11 μm. The histogram represents the experimental droplet size distribution. The height of each vertical bar represents the percentage of the droplets that fall into a particular size bin of a 1 μm increment.

Droplet sizes measured with the witness plates are comparable with the measurements from the Mie scattering diagnostic. Experimental configurations for the data shown in Fig. 12 and for the 6 kV data shown in Fig. 11 are similar. The primary difference is the 290 V/mm electric field for the data in Fig. 12, which is generated by applying a 2.9 kV over a 10 mm grid distance, and the 300 V/mm electric field for the 6 kV data in Fig. 11 is generated by applying a 6 kV over a 20 mm grid distance. The working liquids are also different. Tap water is used in the experiment in Fig. 11, compared with ZnO nanoparticle dispersion in tap water, used in the experiment in Fig. 12. Because of the presence of solid particles in the working liquid, the nozzle vibration power is increased to 0.8 W to maintain a stable production of spray. However, based on the Mie scattering measurements, such a small vibration power change should not have a significant impact on the spray particle sizes. The Mie scattering diagnostic measures a 30.0 μm average droplet size with a 20.5 μm FWHM for the 6 kV data in Fig. 11. These measured values compare to the 20 μm average droplet size and 11 μm FWHM for the witness plate measurements. There are several factors that can contribute to the discrepancy between the Mie scattering diagnostic and the AFM results. The thick rim, as shown in Fig. 13, must contain some ZnO particles, which are not included in the calculation of the droplet size. If included, the AFM results are closer to that from the Mie scattering diagnostic. Other factors, including the relatively small sample population and the irregular shapes of the nanoparticle thin films (compared with perfectly round shape assumed for the droplet size calculation), can also contribute to a statistical fit error for the data in Fig. 14.

Figure 15 shows an optical image of the nanoparticle film deposited on a glass slide for a low power operating condition of the

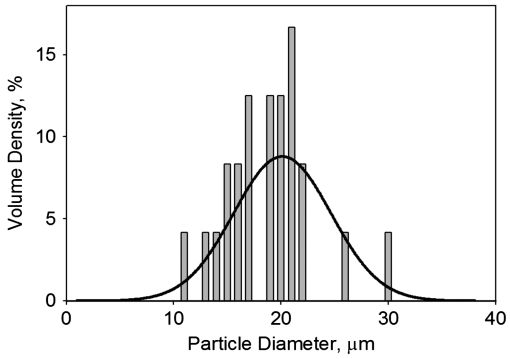

Fig. 14 Droplet size distribution for the same conditions as used in Fig. 12, with a Gaussian distribution fit to the experimental data.

UAE system. All conditions are the same as in Fig. 12, except that the liquid flow rate is 1 ml/hr and the nozzle vibration power is 0.4 W, which is the lowest power possible to produce an electrospray at this experimental condition. The liquid flow rate is set to 1 ml/hr to avoid liquid accumulation at the nozzle tip. The charged capillary standing waves are maintained at the critical stable condition, and the applied electric field dominates the atomization. For this operating condition, 60 thin nanoparticle film samples are examined. The average diameter of the thin films is 33 μm, and the standard deviation is 10 μm. Figure 16 shows the AFM results. The average nanoparticle film thickness is 69 nm.

Figure 17 shows the droplet size distribution based on Eq. (22). The average droplet diameter is 14 μm, and the associated standard deviation is 2 μm. The histogram represents the experimental droplet size distribution. The experimental data are fit with a Gaussian distribution, corresponding to an FWHM of 6 μm.

The low liquid flow rate needed to maintain the critical stable condition generates an electrospray with a density too low to be detected by the Mie scattering diagnostic. No direct comparison between the two measurement methods is possible for this condition.

The nanoparticle films in Fig. 15 are smaller than the films in Fig. 12. The size difference is also evident from the statistical data of the calculated droplet sizes shown in Figs. 14 and 17. The distribution in Fig. 17 shows a more uniform (narrower) size distribution than the distribution in Fig. 14, with the FWHM reduced from 11 μm in Fig. 14 to 6 μm in Fig. 17. The trend in the electrospray characteristics shown in Figs. 12 and 15 is consistent with the Mie scattering data shown in Fig. 11 and Table 1 (i.e., when the UAE operates in the electric-field-dominant regime, smaller and more uniformly charged particles are produced). The operating parameters used for Fig. 12 produce an electrospray, in which vibration still has a significant effect on the atomization. However, the operating parameters used for Fig. 15 produce an electrospray, in which the electric field dominates the atomization and vibration has a reduced effect.

The films in Fig. 15 are more nearly round, as compared with the irregular film shapes in Fig. 12. Surface tension likely keeps the smaller droplets nearly round after the droplets impact the witness plate. When larger droplets strike the witness plate, the impact force is more significant when compared with the surface tension, and the footprint of the droplet is more irregular. The same effect results in thicker average films in the smaller droplets, as shown in Fig. 16, which is 69 nm compared to 46 nm in Fig. 13.

The size and charge-to-mass ratio of the electrospray are related according to the Rayleigh stability criterion. The smallest droplets produced by the experimental UAE system with a 120 kHz nozzle have an average diameter of 14 μm, as shown in Fig. 17. The maximum charge-to-mass ratio given by Eq. (10) is 0.26 C/kg. The electrospray produced by the cone-jet mode has main droplets that

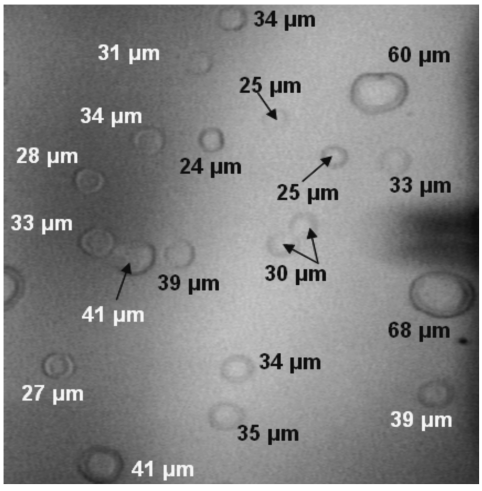

Fig. 15 ZnO nanoparticle thin films deposited on a glass slide witness plate.

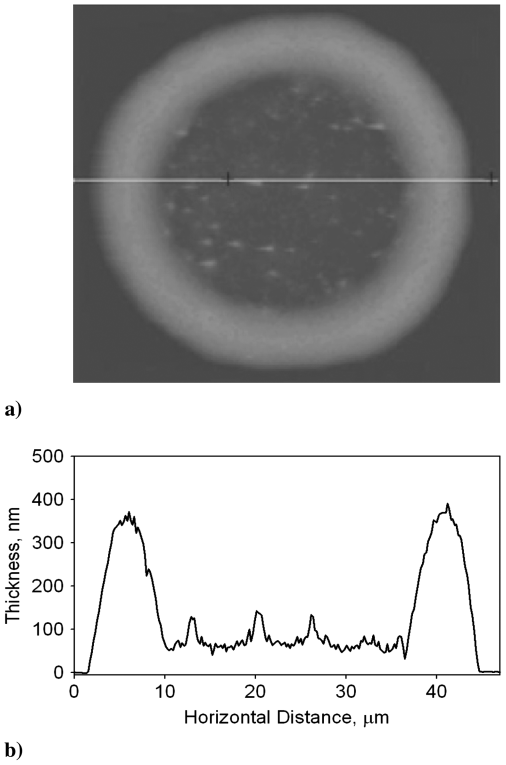

Fig. 16 Sample AFM results for the 39 μm diameter film in Fig. 15: a) AFM image of the thin nanoparticle film; and b) thickness of the nanoparticle thin film along the center chord through the nanoparticle thin film.

are typically on the order of a few microns in diameter and have charge-to-mass ratios in the range of 1 to 100 C/kg [11]. The experimental UAE system in this study produces larger charged droplets with lower charge-to-mass ratios. A UAE system operating at a higher vibration frequency should produce smaller droplet sizes with higher charge-to-mass ratios. An electrospray with an average spray droplet size of 1 μm in diameter requires capillary waves with a wavelength of approximately 3 to 5 μm. Capillary waves with this wavelength in water can be achieved by using an ultrasonic nozzle operating at a frequency of approximately 3.2 MHz. Control of particle size and distribution width has been experimentally demonstrated. Direct production of nanoparticles is theoretically achievable, as shown in Sec. III.

The ultimate goal of the UAE concept is to produce monodisperse, uniformly charged nanoparticles (droplets) at a high mass flow rate, which is useful for high performance electric space propulsion and other nanotechnology areas. Because of the high density of the charged capillary waves, the UAE system (which is linearly scalable) has the potential to produce charged particles at much higher flow rates than traditional electrospraying methods, whereas the Taylor

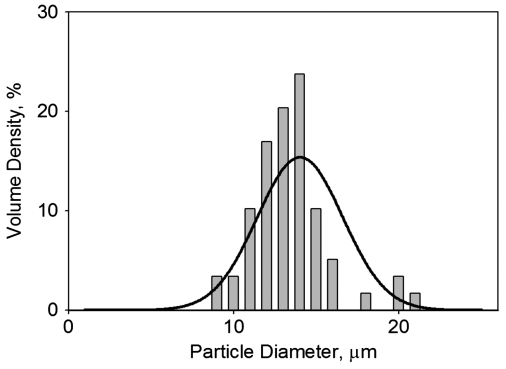

Fig. 17 Droplet size distribution for the same conditions as used in Fig. 15, with a Gaussian distribution fit to the experimental data.

cones are supported by individual capillary hardware (which inherently limits the density). The high mass flow rate distinguishes the UAE from other technologies and makes it appropriate for high performance, high-thruster density space propulsion applications. Using charged nanoparticles as the propellant, an electrostatic thruster can potentially achieve higher thruster density than other types of electric thrusters. For example, assuming the propellant is fully charged formamide droplets of 40 nm in diameter, a specific impulse of 1200 s and a thruster density of approximately 200 $\mathrm{N/m^2}$ can be achieved [19], which is substantially higher than the existing colloid thrusters [9–13].

VI. Conclusions

A method of producing a high flux of nearly monodisperse electrospray using charged capillary standing waves at a critical stable condition is presented. Theoretical analysis indicates that a Taylor cone can be supported by a capillary standing wave with proper wavelength and curvature at the wave tip. Charged droplets are produced when internal forces in the wave are imbalanced, specifically, an imbalance between the surface tension and the combined inertial and electrostatic forces. The size and charge-to-mass ratio of spray particles are directly related to the applied electric field. Experimental results reveal two operating regimes for the UAE method: vibration-dominated and electric-field-dominated. The transition occurs when the electrostatic force (due to the electric field) is significantly larger than the inertial force (due to vibration). Operating in the electric-field-dominated regime produces an electrospray that has smaller and more uniform droplets and higher charge-to-mass ratio. Particle size and charge-to-mass ratio can be controlled by adjusting the vibration frequency, the amplitude, and the intensity of the applied electric field. Smaller particle sizes are produced by standing capillary waves with shorter wavelengths that result from higher frequency vibrations. An electrospray source based on the UAE method has applications to electrostatic space thrusters and other applications, such as nanoparticle coating, because the produced electrospray is an aerosol of nearly monodisperse charged nanoparticles.

Acknowledgments

The authors are grateful to G. Shah and R. Golingo for their help with the experimental studies. Part of this work was conducted at the University of Washington NanoTech User Facility, a member of the NSF National Nanotechnology Infrastructure Network.

References

[1] Jahn, R. G., *Physics of Electric Propulsion*, McGraw–Hill, New York, 1968, pp. 188–191.

[2] Liu, H., *Science and Engineering of Droplets, Fundamentals and Application*, Noyes Publications/William Andrew, New York, 2000, pp. 49–59.

[3] Applications and Products, National Nanotechnology Initiative, http://www.nano.gov/html/facts/nanoapplicationsandproducts.html [retrieved 15 Aug. 2008].

[4] Bailey, A. G., *Electrostatic Spraying of Liquids*, Wiley, New York, 1988, Chap. 1.

[5] Fernandez La Mora, J., and Loscdertales, I. G., "The Current Emitted by Highly Conducting Taylor Cones," *Journal of Fluid Mechanics*, Vol. 260, Feb. 1994, pp. 155–184. doi:10.1017/S0022112094003472

[6] Cherney, L. T., "Structure of Taylor Cone-Jets: Limit of Low Flow Rates," *Journal of Fluid Mechanics*, Vol. 378, Jan. 1999, pp. 167–196. doi:10.1017/S002211209800319X

[7] De Juan, L. E., and Fernandez La Mora, J., "Charge and Size Distribution of Electrospray Drops," *Journal of Colloid and Interface Science*, Vol. 186, No. 2, 1997, pp. 280–293. doi:10.1006/jcis.1996.4654

[8] Gamero-Castano, M., and Hruby, V., "Electric Measurements of Charged Sprays Emitted by Cone-Jets," *Journal of Fluid Mechanics*, Vol. 459, May 2002, pp. 245–276. doi:10.1017/S002211200200798X

[9] Gamero-Castano, M., and Hruby, V., "Characterization of a Colloid Thruster Performing in the Micro-Newton Thrust Range," *27th International Electric Propulsion Conference*, IEPC-01-282, Electric Rocket Propulsion Society, Fairview Park, OH, 2001.

[10] Gamero-Castano, M., "Characterization of a Six-Emitter Colloid Thruster Using a Torsional Balance," *Journal of Propulsion and Power*, Vol. 20, No. 4, 2004, pp. 736–741. doi:10.2514/1.2470

[11] Gamero-Castano, M., and Hruby, V., "Electrospray as a Source of Nanoparticles for Efficient Colloid Thrusters," *Journal of Propulsion and Power*, Vol. 17, No. 5, 2001, pp. 977–987. doi:10.2514/2.5858

[12] Alexander, M. S., Stark, J., Smith, K. L., Stevens, B., and Kent, B., "Electrospray Performance of Microfabricated Colloid Thruster Arrays," *Journal of Propulsion and Power*, Vol. 22, No. 3, 2006, pp. 620–627. doi:10.2514/1.15190

[13] Velasquez-Garcia, L. F., Martinez-Sanchez, M., and Akinwande, A. I., "Two-Dimensional Micro-Fabricated Colloid Thruster Arrays," 40th AIAA/ASME/SAE/ASEE Joint Propulsion Conference and Exhibit, AIAA Paper 2004-3595, July 2004.

[14] Zeleny, J., "The Electrical Discharge from Liquid Points, and a Hydrostatic Method of Measuring the Electric Intensity at Their Surfaces," *Physical Review Letters*, Vol. 3, No. 2, 1914, pp. 69–91. doi:10.1103/PhysRev.3.69

[15] Zeleny, J., "Instability of Electrified Liquid Surfaces," *Physical Review Letters*, Vol. 10, No. 1, 1917, pp. 1–6. doi:10.1103/PhysRev.10.1

[16] Taylor, G. I., "Disintegration of Water Drops in an Electric Field," *Proceedings of the Royal Society of London A*, Vol. 280, No. 1382, 1964, pp. 383–397. doi:10.1098/rspa.1964.0151

[17] Okuda, K., and Kelly, A. J., "Electrostatic Atomization: Experiment, Theory and Industrial Application," *Physics of Plasmas*, Vol. 3, No. 5, 1996, pp. 2191–2196. doi:10.1063/1.871674

[18] Song, W., and Shumlak, U., "Charged Nanoparticle Source for High Thrust Level Colloid Thruster," *Journal of Propulsion and Power*, Vol. 24, No. 1, 2008, pp. 139–141. doi:10.2514/1.27275

[19] Song, W., "Ultrasonically Aided Electrospray Source for Monodisperse, Charged Particles," Ph.D. Dissertation, Univ. of Washington, Seattle, WA, May 2008.

[20] Yule, A. J., and Al-Suleimani, Y., "On Droplet Formation from Capillary Waves on a Vibrating Surface," *Proceedings of the Royal Society of London A*, Vol. 456, No. 1997, 2000, pp. 1069–1085. doi:10.1098/rspa.2000.0551

[21] Griffiths, D. J., *Introduction to Electrodynamics*, Prentice–Hall, Englewood Cliffs, NJ, 1981, pp. 90–91.

[22] Lord Rayleigh, "On the Instability of Jets," *Proceedings of the London Mathematical Society*, Vol. s1–10, No. 1, 1878, pp. 4–13. doi:10.1112/plms/s1-10.1.4

[23] Weiner, I., Rust, M., and Donnelly, T. D., "Particle Size Determination: An Undergraduate Lab in Mie Scattering," *American Journal of Physics*, Vol. 69, No. 2, 2001, pp. 129–136. doi:10.1119/1.1311785

[24] Chiu, Y., Austin, B. L., Dressler, R. A., Levandier, D., Murray, P. T., Lozano, P., and Martinez-Sanchez, M., "Mass Spectrometric Analysis of Colloid Thruster Ion Emission from Selected Propellants," *Journal of Propulsion and Power*, Vol. 21, No. 3, 2005, pp. 416–423. doi:10.2514/1.9690

A. Gallimore
Associate Editor